Title

RNA-binding protein isoforms ZAP-S and ZAP-L have distinct antiviral and immune resolution functions

Journal

Nature Immunology, 20(12)

ISSN

1529-2908

Authors

Schwerk, Johannes
Soveg, Frank W
Ryan, Andrew P
et al.

Publication Date

2019-12-01

DOI

10.1038/s41590-019-0527-6

Peer reviewed

HHS Public Access

Author manuscript

Nat Immunol. Author manuscript; available in PMC 2020 December 01.

Published in final edited form as:

Nat Immunol. 2019 December ; 20(12): 1610–1620. doi:10.1038/s41590-019-0527-6.

RNA-binding protein isoforms ZAP-S and ZAP-L have distinct antiviral and immune resolution functions

Johannes Schwerk[1,6], **Frank W. Soveg**[1,6], **Andrew P. Ryan**[2], **Kerri R. Thomas**[1], **Lauren D. Hatfield**[1], **Snehal Ozarkar**[1], **Adriana Forero**[1], **Alison M. Kell**[1], **Justin A. Roby**[1], **Lomon So**[1,3], **Jennifer L. Hyde**[4], **Michael Gale Jr.**[1,5], **Matthew D. Daugherty**[2,7], **Ram Savan**[1,5,7]

[1]Department of Immunology, School of Medicine, University of Washington, Seattle, Washington, USA

[2]Section of Molecular Biology, Division of Biological Sciences, University of California San Diego, La Jolla, California, USA

[3]Immunology Program, Benaroya Research Institute at Virginia Mason, Seattle, Washington, USA

[4]Department of Microbiology, School of Medicine, University of Washington, Seattle, Washington, USA

[5]Center for Innate Immunity and Immune Disease, University of Washington, Seattle, Washington, USA

Abstract

The initial response to viral infection is anticipatory, with host antiviral restriction factors and pathogen sensors constantly surveying the cell to rapidly mount an antiviral response through the synthesis and downstream activity of interferons. After pathogen clearance, the host's ability to resolve this antiviral response and return to homeostasis is critical. Here, we found that isoforms of the RNA-binding protein ZAP functioned as a direct antiviral restriction factor and as an interferon-resolution factor. The short isoform of ZAP bound to and mediated the degradation of several host interferon mRNAs, and thus acted as a negative feedback regulator of the interferon response. In contrast, the long isoform of ZAP had antiviral functions and did not regulate interferon. The two isoforms contained identical RNA-targeting domains, but differences in their intracellular localization modulated specificity for host versus viral RNA, which resulted in opposing effects on viral replication during the innate immune response.

Cells infected with viruses mount an antiviral response to block viral replication, alert neighboring cells to limit viral spread and ultimately clear the infection. Cell-intrinsic antiviral restriction factors are the first line of defense that prevent a virus from establishing a productive infection. Viral pathogen associated molecular patterns (PAMPs) that are sensed by host pattern recognition receptors (PRRs) trigger a signaling cascade that induces

[7]Corresponding authors: Ram Savan (savanram@uw.edu) and Matthew D. Daugherty (mddaugherty@ucsd.edu).

AUTHOR CONTRIBUTIONS

J.S., F.W.S., M.G., M.D.D., and R.S. designed the study; R.S. directed the study. J.S., F.W.S., A.P.R., K.R.T., L.D.H., S.O., A.F., A.M.K., J.A.R., L.S. and J.L.H. performed experiments and analyzed the data. J.S., M.D.D., and R.S. wrote the manuscript.

[6]Equal contribution

the synthesis of antiviral factors including type I and III interferons (IFNs). These IFNs are then secreted to induce an antiviral program in neighboring cells via activation of hundreds of IFN-stimulated genes (ISGs)[1], including factors that directly limit viral replication such as APOBECs, Mx and IFITs[2, 3, 4]. Although a potent inhibitor of viral replication, the IFN response must be tightly regulated to prevent tissue damage. Despite the importance of returning to homeostasis post-infection, the mechanistic details underlying the attenuation of IFN responses after infection are poorly understood. One proposed mechanism for the resolution of IFN responses is the post-transcriptional regulation of immune genes. Specifically, the mRNAs of IFN and cytokines contain elements encoded within the 3′UTR, such as microRNA binding sites and motifs for RNA-binding proteins (RBPs), that can destabilize mRNA[5, 6, 7, 8]. However, the RBPs that mediate clearance of IFN mRNAs have remained unknown.

The antiviral restriction factor ZAP (also known as PARP13; gene name *ZC3HAV1*) is an RNA-binding protein that targets viral RNA (vRNA) to inhibit viral replication. Its antiviral properties extend for several classes of viruses, including alphaviruses, filoviruses and retroviruses[9, 10, 11, 12]. ZAP contains tandem zinc-finger motifs that bind vRNA and shuttle it to the exosome for degradation[13, 14]. Early studies were carried out under the assumption that only one isoform of ZAP exists. Subsequent studies identified a long isoform of ZAP, named ZAP-L, generated from the same *ZC3HAV1* gene and which contains an additional C-terminal catalytically inactive poly ADP-ribose polymerase (PARP) domain[15, 16]. Because both ZAP-L and ZAP-S contain identical N-terminal zinc-finger motifs that can bind RNA, it is unclear if the isoforms play independent or overlapping roles in coordinating the innate antiviral immune response.

In this study, we show that ZAP-S and ZAP-L have distinct functions during the innate antiviral immune response. ZAP-S was induced late after immune activation and bound and negatively regulated *IFN* mRNA to blunt immune responses downstream of IFN. In contrast, the ZAP-L isoform was expressed constitutively and was the primary antiviral effector. We found that differential subcellular localization of the two isoforms, mediated by the presence or absence of a C-terminal prenylation motif, was the principal determinant of the distinct activities of ZAPL and ZAP-S. Our data provides mechanistic insights into the distinct localization and expression kinetics of ZAP isoforms, which conferred differential target-RNA specificity and opposing functions during viral infection.

RESULTS

ZAP-S interacts with the 3′UTR of *IFN* mRNAs

AU-rich elements (AREs) in the 3′UTR of *IFNL3* are required for the rapid decay of the *IFNL3* mRNA[6]. To identify the RBPs that bind to the ARE of *IFNL3* specifically, we performed a mass-spectrometry screen for candidate proteins that are recruited to the 3′UTR of wild-type *IFNL3* mRNA (WT *IFNL3*), but not to the 3′UTR in which the AREs were mutated (ΔAREs; AUUUA>AUCUA). Biotinylated WT *IFNL3* or ΔAREs 3′UTRs (Fig. 1a) were incubated with whole cell lysates from HepG2 hepatoma cells, streptavidin-affinity purified and subjected to mass spectrometry. Of the candidate proteins that bound to either *IFNL3* 3′UTR, ZAP-S showed the highest relative preference to bind to WT *IFNL3* (Fig.

1b). Next, Huh7 cells were transfected with either FLAG-tagged ZAP-S or ZAP-L and stimulated with the RIG-I ligand poly U/UC RNA to induce expression of endogenous *IFNL3* mRNA (Fig. 1c). FLAG-tagged ZAP-S or ZAP-L were then affinity-purified, and the co-precipitated total RNA was probed for *IFNL3* mRNA by qPCR. *IFNL3* mRNA was significantly enriched in the ZAP-S RNA immunoprecipitation (RIP) fraction, but not in the ZAP-L RIP fraction, even though ZAP-L and ZAP-S have identical RNA-binding zinc-finger motifs[15] (Fig. 1c,d). Because *IFN* genes share similar instability motifs, we also tested if ZAP-S bound to other *IFN* mRNAs. We observed enrichment of *IFNL1*, *IFNL2* and *IFNB* mRNA in the ZAP-S RIP fractions, while ZAP-L RIP fractions did not show significant enrichment of *IFN* mRNA over IgG control (Fig. 1d). RIP under UV-crosslinking conditions, to exclude a potential post-lysis re-assortment of ZAP and its target RNAs, indicated enrichment of *IFN* mRNAs in the ZAP-S RIP fractions compared to ZAP-L and empty vector (EV) RIP fractions (Supplementary Fig. 1a). We next performed RIP of *IFN* mRNA and endogenous ZAP in Huh7 hepatocytes. In Huh7 cells lacking functional type I IFN receptor (*IFNAR1*$^{-/-}$), which did not express ZAP-S after stimulation with poly U/UC RNA, less *IFNB* mRNA was pulled down compared to wild-type Huh7 cells, which expressed ZAP-S (Supplementary Fig. 1b). These data suggested that ZAP-S, but not ZAP-L, was specifically recruited to several host immune genes by recognition of 3′UTR motifs that contain AU-rich elements.

ZAP-S induction is delayed and is dependent on IFN signaling

Because induction of ZAP-S is dependent on type I IFN signaling[17, 18, 19], we assessed the expression kinetics of ZAP-S and ZAP-L upon stimulation of Huh7 hepatocytes with poly U/UC RNA and IFN. While ZAP-L protein was expressed constitutively in mock-transfected wild-type Huh7 cells, expression of ZAP-S protein was detected no sooner than 24 h post stimulation with poly U/UC RNA (Fig. 1e). We observed reduced expression of ZAP-S in *IFNAR1*$^{-/-}$ Huh7 cells compared to Huh7 wild-type cells (Fig. 1e), indicating that induction of ZAP-S was dependent on type I IFN receptor signaling. Stimulation of *IRF3*$^{-/-}$ Huh7 cells with poly U/UC RNA did not induce the expression of ZAP-S protein at 48 h after stimulation, whereas stimulation of *IRF3*$^{-/-}$ Huh7 cells with recombinant IFN-α2 led to robust expression of ZAP-S at 48 h (Fig. 1f), indicating that expression of ZAP-S upon virus-like PAMP stimulation was IRF3-dependent. Furthermore, stimulation of wild-type and *STAT1*$^{-/-}$ PH5CH8 hepatocytes cells with recombinant IFN-β, IFN-λ3 and IFN-γ led to ZAP-S expression in wild-type PH5CH8 cells, but not in *STAT1*$^{-/-}$ PH5CH8 cells (Fig. 1g,h), indicating that expression of ZAP-S was dependent on intact STAT1 signaling. These data showed that ZAP-L was constitutively expressed, while the expression of ZAP-S occurred no sooner than 24 h after stimulation and was dependent on IFN signaling.

CSTF2-mediated alternative polyadenylation generates ZAP-S

Alternative splicing was proposed to mediate the expression of ZAP-L and ZAP-S from the same gene[15]. We found that the ZAP-S mRNA utilized the first 694 base pairs of the intron between exons 9 and 10 as a 3′UTR and that this 3′UTR deployed a weaker non-canonical polyadenylation signal, AGUAAA (Fig. 2a). Because the induction of ZAP-S expression was dependent on type I IFN receptor signaling, we designed a ZAP-S splicing PCR assay that allowed us to detect the usage of the proximal non-canonical polyadenylation signal of

ZAP-S, compared to skipping of this polyadenylation signal and expression of ZAP-L. Treatment of wild-type Huh7 cells with recombinant IFN-β led to a strong increase in usage of the alternative polyadenylation signal and 3′UTR of ZAP-S, which was absent in untreated wild-type Huh7 cells and IFN-β-treated *IFNAR1*$^{-/-}$ Huh7 cells (Fig. 2b). ZAP-L expression was independent of type I IFN signaling (Fig. 2b). Additionally, qPCR using isoform-specific ZAP probes in wild-type and IFNAR1−/− Huh7 cells after stimulation with IFN-β confirmed the validity of the ZAP-S splicing PCR assay (Fig. 2c).

We next investigated the factors that bound to the 3′UTR of ZAP-S and induced its expression. Analysis of the ZAP-S 3′UTR indicated a conserved upstream element (USE) and a downstream element (DSE), which are required for recruitment of the cleavage factor CSTF2 (also known as CstF-64) and the CSTF2-dependent processing of weak non-canonical polyadenylation signals[20, 21, 22], flanking the non-canonical polyadenylation signal of ZAP-S. We used the ZAP-S splicing PCR assay to test if CSTF2 was involved in the generation of ZAP-S in Huh7 cells through alternative polyadenylation cells upon knockdown of CSFT2 and treatment with IFN-β. Usage of the non-canonical polyadenylation signal in ZAP-S was reduced in Huh7 cells upon siRNA-mediated knockdown of CSTF2 compared to non-targeting control (NC) siRNA, whereas expression of ZAP-L in Huh7 cells was unaffected by the knockdown of CSTF2 compared to non-targeting control (NC) siRNA (Fig. 2d,e). More importantly, ZAP-S protein expression was decreased in Huh7 wild-type cells upon siRNA-mediated knockdown of CSTF2 and stimulation with recombinant IFN-β, compared to non-targeting control (NC) siRNA, whereas expression of ZAP-L protein remained unaltered (Fig. 2f). Collectively, these data indicated that the ZAP-S isoform was generated by alternative polyadenylation through a mechanism that involved type I IFN signaling and the polyadenylation factor CSTF2.

ZAP-deficient cells have a higher and more prolonged IFN response

ZAP recruits target viral RNAs to the exosome machinery to mediate decay of bound viral RNAs[12, 14, 23]. To test whether ZAP-S deployed a similar decay machinery to dampen the IFN response, we generated ZAP-deficient Huh7 hepatoma cells by using the CRISPR/Cas9 technology and guide RNA targeting the first exon of ZAP, which is required for the expression of both ZAP isoforms, and isolated single ZAP isoforms-deficient Huh7 cell clones (hereafter ZAP KO Huh7 cells) from a heterogeneous cell population (Fig. 3a and Supplementary Fig. 2a e). ZAP KO Huh7 cells had increased expression of *IFNB*, *IFNL2* and *IFNL3* mRNA after stimulation with poly U/UC RNA compared to wild-type Huh7 cells (Fig. 3b), suggesting ZAP KO Huh7 cells could not control IFN production upon a virus-like insult. To test whether ZAP was critical to resolve the IFN response, we performed a time course analysis of IFN expression after stimulation of wild-type and ZAP KO Huh7 cells with poly U/UC RNA. To exclude the effects of differential uptake of the stimulus, cells were pulsed with transfected poly U/UC RNA for 2 h. While induction of *IFNB* mRNA was maximal at 12 h and resolved at 36 h post stimulation in wild-type Huh7 cells, the ZAP KO Huh7 cells showed about 20-fold elevated peak expression at 12 h and delayed resolution of *IFNB* mRNA between 12 and 36 h compared to wild-type Huh7 cells (Fig. 3c). Similarly, expression of *IFNL3* mRNA was significantly higher (5-fold) and exhibited delayed resolution between 12 and 36 h in ZAP KO Huh7 cells compared to wild-

type Huh7 cells (Fig. 3c). Sustained and increased expression of *IFN* mRNA was substantiated by the 6 to 16-fold increased expression of ISGs mRNA (*IFIT1* and *ISG15*) at 24 and 48 h after poly U/UC RNA stimulation and ISG protein (ISG15 and RIG-I) 48 h post poly U/UC RNA stimulation in ZAP KO Huh7 cells compared to wild-type cells (Fig. 3d,e). Importantly, the basal expression of RIG-I protein, the cytosolic sensor of poly U/UC RNA, and IRF3 protein were similar between unstimulated wild-type and ZAP KO Huh7 cells (Fig. 3e). Stimulation with recombinant IFN-β did not result in sustained and increased expression of ISG mRNA and protein in ZAP KO Huh7 cells compared to wild-type cells (Fig. 3f,g). Furthermore, polysome fractionation indicated that neither ZAP-S nor ZAP-L interacted with actively translating polyribosomes (Fig. 3h). Treatment of wild-type Huh7 cells with harringtonine, an inhibitor of translation initiation, resulted in the disruption of polyribosomes, as indicated by the polysome traces, and a shift of the ribosomal protein S6 towards the lighter non-polysome fractions (Fig. 3h). ZAP-S and ZAP-L did not co-sediment with S6 in the absence of harringtonine, and a shift in the sedimentation pattern of ZAP-S and ZAP-L was not observed in the presence of harringtonine (Fig. 3h). Furthermore, overexpression of ZAP-S and ZAP-L did not affect the amount of *IFNB* and *HPRT* mRNA loaded on actively translating polyribosomes compared to EV control (Supplementary Fig. 2f), indicating that differences in overall mRNA translation and protein synthesis were not a major contributor to the prolonged, elevated IFN mRNA in ZAP KO Huh7 cells compared to wild-type cells. These experiments indicated that ZAP-S expression promoted the resolution of IFN-mediated immune responses.

ZAP-S and ZAP-L localize to different subcellular compartments

Mouse ZAP-L was shown to be targeted to endolysosomal membranes by a C-terminal CaaX (‘C’ cysteine, ‘a’ aliphatic amino acid, ‘X’ variable amino acid) motif that can be prenylated by S-farnesyltransferases[24] (Fig. 4a). Prenylation is a post-translational modification that renders proteins hydrophobic, thereby tethering them to membranes[25]. To investigate whether ZAP-S and ZAP-L occupied distinct subcellular compartments, that would give them differential access to unique pools of RNA, we carried out immunofluorescence staining and confocal microscopy of ZAP isoforms in ZAP KO Huh7 cells co-transfected with Myc-tagged ZAP-S and FLAG-tagged ZAP-L. Myc-ZAP-S had a diffuse cytoplasmic distribution, while FLAG-ZAP-L aggregated in condensed foci, with no overlap between Myc-ZAP-S and FLAG-ZAP-L (Fig. 4b). Next we used structured illumination microscopy (SIM), a super-resolution microscopy which doubles the lateral resolution over conventional confocal laser scanning microscopy[26], to obtain higher resolution of ZAP isoform localization. SIM indicated that Myc-ZAP-S and FLAG-ZAPL did not co-localize within ZAP KO Huh7 cells, and that Myc-ZAP-S occupied the cytosolic compartment while FLAG-ZAP-L occupied a population of vesicles (Fig. 4c). Tagless ZAP-S and ZAP-L detected by antibody staining showed similar subcellular distribution in ZAP KO Huh7 cells as their tagged counterparts (Fig. 4d), thereby excluding an influence of the Myc and FLAG tags on the subcellular localization. Staining of wild-type and ZAP KO Huh7 cells confirmed the specificity of the antibody for endogenous ZAP (Supplementary Fig. 3a). To identify the subcellular localization of human ZAP-L, we co-expressed tagless ZAP-L and ZAP-S along with mCherry-tagged organelle markers for LAMP1 (lysosome), Rab5 (early endosome), Rab7 (late endosome), Sec61β (endoplasmic reticulum), PTS1

(peroxisome) and COX8 (mitochondria). Immunofluorescence staining showed that tagless ZAP-L, but not tagless ZAP-S, co-localized with the lysosomal marker LAMP1 (Fig. 4e,f), and also co-localized with Rab5$^+$ and Rab7$^+$ vesicles in the endosomal pathway (Fig. 4f, Supplementary Fig. 4a,b and Table 1). SIM indicated that ZAP-L specifically localized to the membranes of LAMP1$^+$ endolysosomes. Although ZAP was in proximity to the endoplasmic reticulum (ER), we did not observe isoform-specificity to the co-localization of tagless ZAP-L or tagless ZAP-S with the ER by immunofluorescence microscopy (Supplementary Fig. 5a,b). We did not observe the cosedimentation of ZAP-S and the ER-marker calnexin in a membrane flotation assay (Supplementary Fig. 5c). Furthermore, we did not observe the co-localization of tagless ZAP-L with peroxisomes or mitochondria (Supplementary Fig. 5d,e and Table 1). To ask whether the C-terminal CaaX motif was necessary and sufficient for the differential subcellular localization of ZAP-L and ZAP-S, we generated two expression constructs in which we either mutated the ZAP-L CaaX motif (ZAP-L SVIS) or added a CaaX motif to ZAP-S (ZAP-S+CVIS) (Fig. 4a). When expressed in ZAP KO Huh7 cells, ZAP-L SVIS did not overlap with the endolysosomal markers Rab5, Rab7 and LAMP1 and had a diffuse cytoplasmic distribution, which resembled the cytosolic localization of wild-type ZAP-S (WT ZAP-S) (Fig. 4d–f and Supplementary Fig. 4a,b). Expression of ZAP-S+CVIS in ZAP KO Huh7 cells led to formation of distinct foci positive for LAMP1, Rab5 and Rab7 staining, as seen for WT ZAP-L (Fig. 4e,f and Supplementary Fig. 3a, 4a,b), indicating a gain of endolysosomal localization through the addition of a CaaX motif to the C-terminus of ZAP-S. To confirm the immunofluorescence data, we carried out subcellular fractionation of ZAP KO Huh7 cells overexpressing WT ZAP-S, WT ZAP-L, ZAP-L SVIS or ZAP-S+CVIS. WT ZAP-S and ZAP-L SVIS were detected in the cytosol, whereas little to no WT ZAP-L or ZAP-S+CVIS were detected in the cytosol (Supplementary Fig. 3b), consistent with our microscopy data. This data shows that absence of presence of the CaaX motif determines the differential subcellular localization of ZAP-S and ZAP-L isoforms.

ZAP-L targets alphavirus RNA at viral replication sites

ZAP has strong antiviral activity against members of the *Alphavirus* genus of the *Togaviridae* family[9, 15, 27] and overexpression of ZAP-L inhibits alphaviruses to a greater extent than ZAP-S[15,24]. To ask whether ZAP showed isoform-specific localization to the replication sites of the alphavirus Sindbis virus (SINV), we infected ZAP KO Huh7 cells overexpressing tagless ZAP-L or ZAP-S with SINV strain Toto and performed immunofluorescence staining of ZAP and SINV dsRNA replication intermediates. ZAP-dense foci formed around SINV dsRNA in ZAP-L-overexpressing ZAP KO Huh7 cells (Fig. 5a). ZAP KO Huh7 cells overexpressing ZAP-S formed few such foci, which were also smaller in size compared to those formed by ZAP-L (Fig. 5a). To test if endogenous ZAP-L co-localized with SINV replication intermediates, we infected wild-type Huh7 cells with SINV (strains Toto and AR86) and stained for endogenous ZAP and SINV dsRNA replication intermediates 6 h post-infection. Endogenous ZAP-L co-localized with SINV (Toto and AR86) RNA replication intermediates (Fig. 5b). Importantly, endogenous ZAPS was not expressed at this time point (Fig. 5c), indicating that the immunofluorescence signal from ZAP was derived from endogenous ZAP-L only. The co-localization of ZAP-L with SINV RNA occurred at the plasma membrane and in conjunction with G3BP1-positive

stress granules, where SINV, like other alphaviruses, assembles its replication sites[28] (Fig. 5b and Supplementary Fig. 6a,b). To address if the co-localization of ZAP-L with SINV RNA required immune activation by the host cell, we infected *IRF3*$^{-/-}$ Huh7 cells, which do not induce IFN or expression of ZAP-S upon PAMP stimulation or viral infection, with SINV Toto for 6 h. Endogenous ZAP-L co-localized with SINV RNA at the cell membranes of *IRF3*$^{-/-}$ Huh7 cells, similar to wild-type Huh7 cells (Fig. 5d), indicating that endogenous ZAP-L preferentially localized to viral RNA and sites of SINV replication on membranes even in the absence of IRF3-mediated innate immune signaling.

To test if the subcellular localization of the ZAP isoforms influenced their antiviral activity against SINV, we generated doxycycline-inducible HEK 293 cells expressing WT ZAP-S, WT ZAP-L, ZAP-L SVIS or ZAP-S+CVIS and infected them with SINV. Supernatants harvested from WT ZAP-L HEK 293 cells infected with SINV showed a strong inhibition (20,000-fold) of viral replication compared to control EV expressing cells, whereas WT ZAP-S-expressing HEK 293 cells showed a much lower degree of inhibition (60-fold) (Fig. 5e). Expression of ZAP-L SVIS decreased the antiviral activity to levels observed in WT ZAP-S-expressing HEK 293 cells (Fig. 5e), while expression of ZAP-S+CVIS led to increased (2,000-fold) antiviral capacity, although 10-fold less than that induced by WT ZAP-L (Fig. 5e). We also used a replicon-based system for another alphavirus, Semliki Forest virus (SFV)[29], which allowed the expression of increasing amounts of the ZAP expression constructs. Overexpression of WT ZAP-L was the most efficient at blocking SFV replication, with ZAP-S+CVIS the second most inhibitory compared to control cells that did not overexpress a plasmid (Supplementary Fig. 6c). WT ZAP-S and ZAP-L-SVIS were the least inhibitory (Supplementary Fig. 6c). To confirm that the effects observed in the overexpression experiments were relevant in the context of endogenously expressed ZAP isoforms, we used an siRNA approach to selectively knock down ZAP-L or ZAP-S during SINV infection in Huh7 cells. We designed isoform-specific siRNAs that either target the 3′UTR of ZAP-S, which is absent in ZAP-L, or exon 12 in ZAP-L, which is absent in ZAP-S, and confirmed their specificity by immunoblot (Fig. 5f). Knockdown of ZAPL, but not ZAP-S, in Huh7 cells resulted in increased SINV replication (Fig. 5g), indicating that ZAP-L was the major antiviral ZAP isoform during alphavirus infection and that ZAP-S had a minimal role in direct antiviral immunity against alphaviruses. These results indicated that the isoform-specific targeting of viral RNA was due to differences in the subcellular localization of ZAP-S and ZAP-L, which were determined by the presence or absence of the C-terminal CaaX motif and allowed the recruitment of ZAP-L to sites of SINV RNA replication at endolysosomes and the plasma membrane.

ZAP-S, but not ZAP-L, suppresses IFN

To address which ZAP isoform was responsible for the increased expression of *IFN* mRNA in ZAP KO Huh7 cells, we performed isoform-specific ZAP siRNA knockdown experiments. Wild-type Huh7 cells were co-transfected with ZAP-L (exon 12) siRNA or ZAP-S (3’UTR) siRNA and poly U/UC RNA to induce expression of IFN and endogenous ZAP-S protein. Transfection of ZAP-S siRNA led to significantly higher expression of *IFNB*, *IFNL2* and *IFNL3* mRNA compared to non-targeting control (NC) siRNA and ZAP-L siRNA (Fig. 6a,b). IRF3 phosphorylation was similar in ZAP-L, ZAP-S and NC siRNA

transfected cells (Fig. 6a), indicating activation of IRF3 was not affected by knockdown of either ZAP isoform. ZAP-S was reported to co-operate with RIG-I to increase RIG-I-mediated IFN responses in HEK 293 cells[17], but knockdown of ZAP-S led to increased IFNB and IFNL3 mRNA in 293 cells compared to ZAP-L knockdown and NC siRNA upon stimulation with poly U/UC RNA (Supplementary Fig. 7a,b). *TNFA* and *IL6* mRNA harbor AREs in their 3′UTRs. *IL6* mRNA was significantly increased upon ZAP-S knockdown in Huh7 cells, while *TNFA* mRNA was not as affected (Supplementary Fig. 7c), although both *IL6* and *TNF* transcripts are bound by the ZAP-S preferentially compared to ZAP-L or EV control (Supplementary Fig. 7d). Overexpression of the phosphomimetic IRF3–5D, which bypasses the signaling pathways upstream of IRF3 activation, led to increased *IFNB* mRNA in ZAP-S-knockdown Huh7 cells compared to ZAP-L-knockdown or NC Huh7 cells (Fig. 6c,d). Stimulation of CAL-1 pDC cells with R848, a TLR7 ligand that signals through IRF7 resulted in increased induction of *IFNL2* and *IFNL3* mRNA in ZAP-S-knockdown CAL-1 cells only (Fig. 6e,f). Additionally, overexpression of IRF1 in ZAP KO Huh7 cells led to significantly increased *IFNB* and *IFNL3* mRNA compared to wild-type Huh7 cells (Supplementary Fig. 7e,f), indicating that the effect of ZAP-S on *IFN* mRNA was not caused by the dysregulation of upstream signaling pathways due to knockdown of ZAP-S. These data indicated that the increased expression of IFN in ZAP KO Huh7 cells was not only specific to the RIG-I-IRF3 signaling axis and that ZAP-L had a minor role in the resolution of IFN responses.

Localization of ZAP isoforms determines binding of *IFN* mRNA

To test if the cytoplasmic localization of ZAP-S determined whether ZAP-S, but not ZAP-L, could target and negatively regulate *IFN* mRNA, we carried out RIP with FLAG-tagged WT ZAP-S, WT ZAP-L, ZAP-L SVIS or ZAP-S+CVIS in ZAP KO Huh7 cells. The disruption of the CaaX motif in the ZAP-L SVIS mutant resulted in increased enrichment of *IFNB* and *IFNL3* mRNA compared to ZAP-L WT, while addition of the CaaX motif to ZAP-S in the ZAP-S+CVIS mutant led to a decrease in its ability to target *IFNB* and *IFNL3* mRNA compared to ZAP-S WT (Fig. 7a), suggesting the CaaX motif was a major determinant for target RNA specificity of ZAP isoforms. To test whether increased IFN expression resulting from a loss of ZAP-S decreased the replication of viruses sensitive to IFN, we used SINV and vesicular stomatitis virus (VSV), both of which are sensitive to the antiviral effects of IFN, while only SINV is sensitive to ZAP-L mediated restriction. We observed elevated SINV replication in the ZAP KO Huh7 cells compared to wild-type Huh7 cells in unstimulated conditions (Fig. 7b), indicating the intrinsic restriction of SINV replication by constitutive ZAP-L. In contrast, we saw no difference in VSV replication between wild-type and ZAP KO Huh7 cells (Fig. 7b), indicating VSV was insensitive to ZAP expression[9]. Both SINV and VSV were more sensitive to IFN-mediated restriction after poly(I:C) stimulation in ZAP KO Huh7 cells compared to wild-type Huh7 cells (Fig. 7b), suggesting that increased IFN levels in ZAP KO Huh7 cells compared to wild-type Huh7 cells have a direct biologically effect on replication of IFN-sensitive viruses. These results show that the isoform-specific binding of ZAP-S to *IFN* mRNA to resolve the antiviral IFN response is determined by its cytosolic localization due to the lack of a C-terminal CaaX motif (Supplementary Fig. 8).

DISCUSSION

Here we found that the innate antiviral immune factor, ZAP has a role in the negative regulation of the immune response. In contrast to the direct antiviral role of the long isoform, ZAP-L, we found that the shorter isoform, ZAP-S, targeted host *IFN* mRNAs to resolve IFN-mediated inflammatory responses. The distinct self-versus non-self RNA recognition by ZAP-S and ZAP-L is linked to differential expression kinetics and subcellular localization, which was determined by prenylation of a C-terminal CaaX motif.

Previous studies have described the antiviral effect of ZAP, mediated through direct binding of viral RNA and RNA degradation[9, 13, 14, 23, 30, 31, 32.] ZAP-S and ZAP-L share an identical N-terminal RNA-binding motif, proposed to be transcribed from the same gene (*ZC3HAV1*) through alternative splicing[15]. Our studies show IFN-induced and CSTF2-dependent alternative polyadenylation leading to alternative last exon usage and generation of ZAP-S. Expression of CSTF2 in immune cells is dependent on the activation status of the cell, with a direct effect on alternative polyadenylation of mRNA[20, 21, 22]. Type I IFN-dependent induction of CSTF2 has been reported[33]. While we did not observe altered expression of CSTF2 after IFN or PAMP stimulation, we do not rule out changes in post-translational modifications of CSTF2 protein, or stimulus-dependent changes in the amounts of CSTF2 co-factors required for its activation.

The motif on the viral RNA that is recognized by ZAP has been elusive, with early papers suggesting that RNA structure-dependent recognition whereas more recent papers indicate that ZAP binds to regions with high CG dinucleotide content[34, 35]. Regardless of the exact target RNA motif, the identical zinc-finger domains of ZAP-S and ZAP-L[34, 36] cannot impart the differential specificity of ZAP isoforms for host *IFN* mRNA sequences. The longer C-terminus of ZAP-L contains a catalytically inactive poly ADP-ribose polymerase (PARP) domain[15] and a functional CaaX prenylation motif[24], which are absent in the ZAP-S isoform. We found that the subcellular localization of ZAP-S and ZAP-L predominantly determined the functional differences observed between the isoforms targeting host and viral RNAs, respectively. Through overexpression and isoform-specific knockdown experiments, we establish that ZAP-L is the dominant antiviral isoform against SINV, which is consistent with previous observations[15, 24]. However, the fact that we could not fully mirror ZAP-L activity by simple re-localization of ZAP-S through the addition of the CaaX motif might be due to the requirement of additional amino acid residues in the C-terminal part of ZAP-L, specifically in the PARP domain, which could provide antiviral functions or additional localization signals. While the PARP domain of ZAP-L lacks the catalytic activity of functional PARPs, the mutations causing PARP inactivity are essential for the antiviral activity of ZAP-L against alphaviruses[37], suggesting that RNA-binding activity might not be the only antiviral mechanism conferred by ZAP[38]. We propose that the primary determinant for higher antiviral activity of ZAP-L over ZAP-S was due to the proximity of ZAP-L to sites of alphavirus replication at the plasma membrane and in endolysosomes with highly abundant vRNA ligands. Prenylation and targeting of ZAP-L to these sites positioned ZAP-L in close proximity to the viral RNA, which might also explain the antiviral specificity of ZAP-L against alphaviruses.

ZAP-S knockdown had specific effects on certain mRNAs and did not affect general mRNA turnover. Although the common feature of *IFNB, IFNL1–3*, *IL6* and *TNFA* mRNAs is the presence of AREs in their 3'UTRs that could be preferentially bound by ZAP-S, we cannot rule out additional motifs aside from the AREs that might determine the specificity of ZAP-S-mediated mRNA regulation. Similar to AREs in human cytokine mRNAs, alphaviruses harbor U-rich elements in their genome. This raises the possibility that the zinc-finger motifs of ZAP-L and ZAP-S target similar motifs in host and viral RNA. The exact RNA structure and motifs recognized by ZAP warrants further investigation.

We observed that the replication of IFN-sensitive viruses was attenuated due to elevated and sustained IFN production in the absence of ZAP-S. This provides a mechanistic explanation for two previous observations in the ZAP literature: First, a previous study using an *in vivo* infection model of ZAP-deficient mice with a neurovirulent Sindbis virus strain (SVNI) reported opposing phenotypes depending on the age of the mice[39]. Suckling ZAP KO mice, which lack a fully developed immune system, were highly susceptible to SVNI[39]. Weanling ZAP-deficient mice, whose immune system is more developed, showed improved survival, along with increased expression of IFN compared to wild-type mice[39]. Based on our data we suggest that suckling ZAP-deficient mice would succumb to infection due to lack of the direct antiviral properties of ZAP-L. Weanling ZAP-deficient mice however could benefit from increased IFN expression due to lack of ZAP-S. Future *in vivo* studies are required to dissect individual contributions of ZAP-L and ZAP-S to innate antiviral immunity.

Second, codons that have undergone recurrent positive selection throughout primate evolution, which might indicate the regions of ZAP that are recognized by viral antagonists, are only found in the catalytically inactive C-terminal PARP domain of ZAP-L[15]. Our data could indicate that ZAP-S might act as an evolutionary 'shield' that protects the remainder of the protein from antagonism. If a viral protein were to prevent ZAP-L function by binding to the N-terminus of the protein, it would also disrupt ZAP-S activity and therefore increase the IFN response. This theory could also explain isoform-specific signatures of positive selection found in other genes. It would be interesting to know if viruses possess mechanisms to selectively increase expression of or stabilize ZAP-S in order to attenuate the IFN response and promote viral replication.

Collectively, our study reveals that the host can diversify the function of RNA-binding protein isoforms to exert unique cellular functions through distinct expression kinetics subcellular localization, highlighting that differential intracellular targeting is an important mechanism controlling the target RNA specificity of RNA-binding proteins.

ONLINE METHODS

Cell culture conditions.

All cells were incubated at 37 °C with 5% CO_2. Huh7, HepG2, PH5CH8 and HEK 293 cells were cultured in DMEM (Sigma) containing 10% heat-inactivated FBS (Atlanta Biologicals) and 1% penicillin-streptomycin-glutamine (Mediatech). BHK cells were cultured in MEM (Sigma) containing 10% heat-inactivated FBS (Atlanta Biologicals) and 1% penicillin-streptomycin-glutamine (Mediatech). CAL-1 cells were grown in RPMI 1640 (Sigma)

containing 10% heat-inactivated FBS (Atlanta Biologicals) and 1% penicillin-streptomycin-glutamine (Mediatech), and supplemented with 2 mM L-Glutamine, 1 mM sodium pyruvate, 10 mM HEPES, 1x MEM NEAA (Corning).

Stimulations.

Recombinant human IFN-α2, IFN-β, IFN-λ3 (PBL Interferon Source) and IFN-γ (Shenandoah Biotechnology) were used at 25–100 ng/ml (IFN-α2), 25–500 IU/ml (IFN-β), 100 ng/ml IFN-λ3 or 5 ng/ml (IFN-γ), respectively. For RIG-I stimulations, poly U/UC RNA was synthesized by *in vitro* transcription as previously described[40]. Poly U/UC RNA was transfected at 0.2–1 μg/ml using *Trans*IT-X2 (Mirus Bio) according to the manufacturer's instructions. Stimulations of TLR3 and TLR7/8 were performed using 10 μg/ml floating poly(I:C) or 1 μg/ml R848 (both InvivoGen) in culture media.

RNA isolation, reverse transcription and quantification of gene expression.

Total RNA was isolated using the NucleoSpin RNA kit (Macherey-Nagel) according to the manufacturer's protocol. cDNA was synthesized from 1 μg total RNA using the QuantiTect RT kit (Qiagen) according to manufacturer's instructions. qPCR was carried out using the ViiA7 qPCR system with *Taq*Man reagents using *Taq*Man primers/probes (Life Technologies) for *IFNB*, *IFNL1*, *ISG15*, *IFIT1*, *MX1*, *OAS1*, *TNFA*, *IL6*, *ZC3HAV1*, *CSTF2*, *HPRT*, *GAPDH* and custom-designed, isoform-specific probes for ZAP-S and ZAP-L (Supplementary Table 1). *Taq*Man primers/probes for *IFNL2* and *IFNL3* were previously designed and tested for specificity[6, 41]. Target gene expression was normalized to *HPRT* or *GAPDH* housekeeping genes.

Western blot.

Cells were lysed in RIPA buffer (+ 1x HALT protease and phosphatase inhibitor and 10–30 μg total protein from whole cell lysates was run on SDS-PAGE and transferred to PVDF membranes (Thermo Scientific). The membranes were probed in 5 % BSA or milk in PBS-T (Phosphate-buffered saline/Tween 20) for ZAP (N3C2, GeneTex), ISG15 (Cell Signaling, #2743), OAS1 (D1W3A, Cell Signaling), RIG-I (Alme-1, AdipoGen), IRF1 (D5E4, Cell Signaling), IRF3 (D83B9, Cell Signaling), phospho-IRF3 (Ser386) (EPR2346, Abcam), STAT1 (42H3, Cell Signaling), phospho-STAT1 (Tyr701) (58D6, Cell Signaling), RPS6 (5G10, Cell Signaling), CSTF2 (Bethyl Laboratories), Calnexin (C5C9, Cell Signaling), FLAG (M2, Sigma), Myc (71D10, Cell Siganling) or β-Actin-HRP (13E5, Cell Signaling). For detailed information about the source of the antibodies and dilutions used please refer to the Life Sciences Reporting Summary.

ZAP siRNA knockdown.

Specific DsiRNAs against ZAP-S and ZAP-L were custom-designed and obtained from Integrated DNA Technologies (IDT) (Supplementary Table 2). DsiRNA against *CSTF2* was obtained from IDT (hs.Ri.CSTF2.13.1). For knockdown experiments, DsiRNA was transfected at 10–20 nM final concentration using *Trans*IT-X2 (Mirus Bio) according to the manufacturer's instructions. Stimulations of cells were performed 24–36 h after DsiRNA transfection. Co-transfections of DsiRNA and poly U/UC RNA or expression plasmids were

performed using *Trans*IT-X2 (Mirus Bio) at a DsiRNA concentration of 10–20 nM. Cells were analyzed 24–42 h post transfection.

Generation of ZAP KO and *IRF3* KO cells.

ZAP targeting guide RNA (gRNA, 5′-GCAACTATTCGCAGTCCGAG-3′) and *IRF3* targeting guide RNA (gRNA, 5′-GTTGGAAGCACGGCCTACGGC-3′) was cloned downstream of the U6 promoter in the pRRLU6-empty-gRNA-MND-Cas9-t2A-Puro vector using In-Fusion enzyme mix (Clontech). Cells were transfected with ZAP- or *IRF3* gRNA-Cas9-expressing plasmids. Cas9-empty-expressing plasmids were transfected as control. 3×10^6 Huh7 cells were seeded onto a 10 cm dish and 10 μg of plasmid was transfected using the $CaPO_4$ transfection kit (Invitrogen) according to the manufacturer's instructions. After 48 h cells were pre-selected by addition of 2 μg/ml puromycin to the media for 2 days. Pre-selected cells were sub-cloned and analyzed for absence of ZAP protein expression by immunoblot upon stimulation with IFNb or transfection of poly U/UC RNA. *IFNAR1* KO cells were generated as previously described[5].

Generation of Flp-In HEK 293T cells expressing doxycycline-inducible ZAP isoforms.

ZAP isoform constructs were cloned into the Flp-In vector pcDNA5/FRT/TO. Flp-In T-REx 293 cells maintained in 5 μg/ml blasticidin were transfected at 70% confluency with ZAP isoform constructs and the vector containing the Flp recombinase pOG44 in a 1:10 molar ratio using *Trans*IT-X2 (Mirus Bio). After one day, cells were transferred to new dishes, and on the following day, hygromycin was added to the cells at a concentration of 100 μg/ml. Following selection, cells were maintained in 5 μg/ml blasticidin and 100 μg/ml hygromycin. For ZAP expression, cells were induced with 500 ng/ml doxycycline.

Mass spectrometry.

IFNL3-WT and *IFNL3*-ΔARE 3′UTR were amplified from constructs containing wildtype (WT) sequences or disrupted ARE (ΔARE) in all three ATTTA motifs; pGL3 constructs described previously[6]. The T7 promoter was incorporated using the following primers: T7-INFL3-F TAATACGACTCACTATAGGGACCCTTCCGCCAGTCATGC and IFNL3-R CAACAAGGATTTCAAAAAGTAGAAAAATAAACATTTTCCTGG. RNA probes were generated using the MAXIscript T7 *In Vitro* Transcription Kit (Ambion) as described by the manufacturer for 1 μg DNA template and were precipitated with ammonium acetate/ethanol. RNA probes were subsequently biotinylated using the RNA 3′End Biotinylation Kit (Pierce) according to manufacturer's instructions for 50 pmol RNA. 1.5×10^6 Huh7 cells were lysed in 100 μl polysome lysis buffer. 2 μg biotinylated RNA probes were incubated with 400 μg protein lysate in 2X TENT buffer (20 mM Tris-HCl, pH 8.0; 2 mM EDTA; 500 mM NaCl; 1% Triton X-100), rocking at room temperature for 1 h. RNA probes were isolated using Dynabeads M-280 Streptavidin. RNA-protein complexes were washed 4 times with ice-cold PBS and eluted in SDS elution buffer (10 mM Tris-HCl, pH 8.0; 1 mM EDTA; 2% SDS), shaking at 1000 rpm for 30 min at 55 °C. Bound proteins were TCA-precipitated and dry protein pellets were frozen at −20 °C until ready for digestion.

Protein pellets from biotinylated RNA pull-downs (~15 μg) were resuspended in 40 μl of 100 mM ammonium bicarbonate + 5% acetonitrile + 8 M urea, subsequently reduced with 4

μl 50 mM DTT, and incubated for 30 min at 56 °C. Cooled samples were then alkylated with 4 μl 100 mM iodoacetamide (IAA) and incubated at room temperature for 30 min in the dark. Unreacted IAA was quenched with 4 μl 50 mM DTT and incubated at room temperature for 15 min in the dark. The protein mixture was diluted 1:5 with 25 mM ammonium bicarbonate + 5% acetonitrile to reduce the concentration of urea to <2 M. 26 μl of 100 mM $CaCl_2$ was added to the mixture before digestion with 7 μl of 0.2 μg/μl trypsin at 37 °C for 4 h. Digestion products were cooled to room temperature before peptide clean-up using C18 Spin Columns (Pierce) according to the manufacturer's instructions. Peptides were eluted in 80 μl of 70% acetonitrile, dried in a SpeedVac for 1.5 h and reconstituted in 10 μl of 5% acetonitrile + 0.1% formic acid. Peptides were loaded onto the ACQUITY UPLC system (Waters), trapped on Magic C18AQ 200Å 5u beads (MichromBioresources PM5/61200/00) and run through an analytical separation column with Magic C18AQ 100Å 5u beads (MichromBioresources PM5/61100/00). Analysis was performed on the LTQ Orbitrap XL (Thermo) mass spectrometer. Peptides were identified using Comet (Dragonfly) and assignments were established using PeptideProphet (ISB). Subsequent protein identification using ProteinProphet (ISB) required a minimum of 2 high confidence peptides (0.01 false discovery rate).

RNA-Immunoprecipitation.

FLAG-tagged ZAP-S and FLAG-tagged ZAP-L expression plasmids were generated by cloning of the ZAP CDS from pcDNA4 huZAP(S) and pcDNA4 huZAP(L) (obtained from Addgene) into the MCS of pEF N-FLAG (gift from Michael A. Davis, UW Immunology). A FLAG-empty vector (EV) was used as negative control for RNA-IP. 4×10^6 Huh7 cells were seeded onto a 10 cm cell culture dish the day before transfection. The next day, 4 μg ZAP-S, ZAP-L, or EV expression plasmid were co-transfected with 2 μg poly U/UC RNA using *Trans*IT-X2 (Mirus Bio) according to the manufacturer's instructions. 24 h after transfection cells were harvested and lysed in RNA-IP lysis buffer (100 mM KCl, 5 mM $MgCl_2$, 10 mM HEPES pH 7.4, 0.5% NP-40, 1 mM DTT, 1x HALT protease inhibitor, 100 U/ml RNasin, 2 mM ribinucleoside-vanadyl complex). Nuclei and debris were removed from cytosolic lysate by centrifugation at 8,000 × g at 4 °C for 10 min. 400 μg protein from cytosolic lysate was incubated with 5 μg anti-FLAG mouse IgG_1 (M2, Sigma) or mouse IgG_1 control over night at 4° C rotating. The next day, 0.75 mg Dynabeads Protein G (Invitrogen) were added and the lysate was incubated for 2 h at 4° C rotating. For RNA-IP of endogenous ZAP, cytosolic lysates were incubated with 10 μg of anti-ZAP antibody (GeneTex) and 1.2 mg Dynabeads Protein G (Invitrogen) were used. After washing, co-precipitated RNA was isolated from IgG_1-protein complexes by chloroform-isoamyl alcohol extraction, reverse transcribed into cDNA (QuantiTect RT kit, Qiagen) and analyzed for mRNA transcripts by qPCR. For UV-crosslinking, cells were irradiated in cold PBS on ice with 120 mJ/cm^2 before cell lysis, using a Stratalinker 1800 (Stratagene).

Confocal immunofluorescence microscopy.

Cells were seeded on type I collagen (Sigma) coated 12 mm coverslips (EMS) and rested overnight. Cells were transfected using *Trans*IT-X2 (Mirus Bio) with expression plasmids encoding respective ZAP isoforms and/or mCherry-tagged organelle markers: Rab5 (Addgene #49201[42]), Rab7A (Addgene #61804[43]), and Sec61β (Addgene #49155[43]) COX8

(Addgene #55102[44]), PTS1 (Addgene #54520), and LAMP-1 (Addgene #55073). mCherry-tagged Rab5, Rab7A, and Sec61β were gifts from Gia Voeltz and COX8, PTS1, and LAMP-1 were gifts from Michael Davidson. At 24 h post-transfection, cells were fixed in 4% PFA/PBS for 10 min at room temperature and then permeabilized with PBS containing 0.1% Triton-X100 for 10 min at room temperature. Permeabilized samples were then blocked for 1 h at room temperature in 3% BSA/PBS and then stained with the following primary antibodies in PBS containing 1% BSA and 0.3% Triton-X100 for 1 h at room temperature: mouse anti-FLAG (Sigma), rabbit anti-Myc (Cell Signaling), rabbit anti-ZAP (GeneTex), mouse J2 anti-dsRNA (Scicons). For immunofluorescence staining of the plasma membrane and stress granules primary anti-E-cadherin (Thermo) and anti-G3BP1 (Abcam) antibodies were used. Cells were washed three times with PBS prior to staining with the following secondary antibodies in PBS containing 1% BSA and 0.3% Triton-X100 for 1 h in the dark at room temperature: goat anti-mouse IgG Alexa Fluor 488, goat anti-rabbit IgG Alexa Fluor 594, and goat anti-rabbit IgG Alexa Fluor 488 (all Thermo Fisher). Samples were washed with PBS three times and then mounted with ProLong Diamond antifade mounting media (Thermo Fisher) with DAPI. Samples were cured in the dark at room temperature prior to imaging. All samples were imaged on a Nikon Eclipse Ti laser scanning confocal microscope using a 60x oil-immersion lens. Images were processed and analyzed using the NIS elements software and Fiji. Quantification of co-localization was performed for 10 cells each, using the Fiji Coloc 2 plugin. Overlays of co-localized pixels were calculated and generated using the Fiji Colocalization Threshold plugin, using Costes auto threshold algorithm to determine true co-localization. For detailed information about the source of the antibodies and dilutions used please refer to the Life Sciences Reporting Summary.

Super-resolution structured illumination microscopy.

All samples were imaged on a DeltaVision OMX SR imaging system (GE Healthcare) using a 60x oil-immersion objective. SIM reconstruction and image alignment was achieved using SoftWoRx. ZAP KO Huh7 cells were seeded on #1.5 high precision glass coverslips (Bioscience Tools) and coated with collagen as described previously. Cells were transfected with Myc-tagged ZAP-S and FLAG-tagged ZAP-L and were stained 24 h post-transfection as previously described. Cells were mounted using ProLong Glass antifade mounting media and cured for 48 h prior to imaging.

Cell fractionations.

For differential subcellular fractionation Huh7 ZAP KO cells were seeded on 10 cm dishes and allowed to settle overnight. Cells were then transfected with expression plasmids encoding either ZAP-S, ZAP-L, ZAP-S+CVIS, or ZAP-L SVIS. At 24 h post transfection, cells were incubated on ice in hypotonic lysis buffer (20 mM HEPES pH 7.4, 10 mM KCl, 2 mM $MgCl_2$, 1 mM EDTA, 1 mM EGTA, 1 mM DTT, 1x HALT protease and phosphatase inhibitor, 3 mM imidazole) for 30 min. Cells were passed through a 27-gauge needle 10 times prior to collection of the soluble cytosolic fraction by spinning down the lysate for 1 h at 100,000 × g in an Optima TL Ultracentrifuge. Whole cell lysates and soluble cytoplasmic fractions were blotted as described previously using antibodies against ZAP (GeneTex), COX IV (Cell Signaling), and α-tubulin (Cell Signaling).

For polyribosome fractionation 1×10^7 Huh7 WT cells were grown on 15 cm dishes and stimulated with 500 IU/ml human recombinant IFN-β for 24 h. Cells were incubated with 5 μg/ml harringtonine (LKT Labs) in PBS for 10 min or with 100 μg/ml cycloheximide (Sigma) in PBS for 5 min at 37 °C with 5% CO_2. Cells were then washed twice in ice-cold PBS and harvested in 500 μl polysome lysis buffer (50 mM Tris-HCl pH 7.5, 100 mM KCl, 12 mM $MgCl_2$, 1% NP-40, 1 mM DTT, 1x HALT protease inhibitor, 100 μg/ml cycloheximide). The lysate was cleared of nuclei and debris by centrifugation at 8,000 × g for 10 min at 4 °C. Supernatants were layered on a 10–50% sucrose gradient and spun at 230,000 × g for 2.5 h at 4 °C. Gradients were then fractionated while continuously monitoring absorbance at 254 nm. 15 μl of each fraction was loaded for Western blot.

Membrane flotation assays were performed as previously described[45], with the following modifications. Briefly, Huh7 WT cells were grown to ~80% confluency in T150 flasks. Cells were harvested and for each condition, 30 million cells were resuspended in PBS containing 0.25 M sucrose and a protease/phosphatase inhibitor cocktail and placed on ice for 30 min. Cells were then lysed on ice with a tight-fitting dounce homogenizer. After 200 passages, lysis efficiency (90%) was assayed by trypan blue staining. Post nuclear lysate was generated by collecting supernatants after centrifugation of the crude lysate at 2,500 × g for 10 min at 4 °C. Protein concentration was determined by BCA and 500 μg of protein was mixed with PBS containing 0.25 M sucrose to a final volume of 2 ml. Samples were then mixed with 2 ml of PBS containing 0.25 M sucrose and 60% (w/v) Histodenz (Sigma) non-ionic density gradient medium. This mixture was then carefully added to a 14 ml ultracentrifuge tube (Beckman) and then 4 ml of PBS containing 0.25 M sucrose and 20% (w/v) Histodenz was carefully overlayed. A final 4 ml of PBS containing 0.25 M sucrose and 10% (w/v) Histodenz was carefully overlayed. Samples were spun down overnight (~16 h) at 4 °C and 209,000 × g in an SW41Ti rotor in an L8–70m ultracentrifuge (Beckman). After spin, 500 μl fractions were taken from the top by careful removal and stored at −80 °C until ready for use.

Ribosome profiling.

1×10^7 Huh7 ZAP KO cells were grown on 15 cm dishes and transfected with plasmids expressing ZAP-S, ZAP-L or empty vector (EV) control. 24 h after plasmid transfection, cells were stimulated with 250 ng/ml poly U/UC RNA for 18 h. Cells were then incubated with 100 μg/ml cycloheximide (Sigma) in PBS for 5 min at 37 °C with 5% CO_2. Cells were washed twice in ice-cold PBS and harvested in 500 μl polysome lysis buffer (50 mM Tris-HCl pH 7.5, 100 mM KCl, 12 mM $MgCl_2$, 1% NP-40, 1 mM DTT, 1x HALT protease inhibitor, 100 μg/ml cycloheximide). The lysate was cleared of nuclei and debris by centrifugation at 8,000 × g for 10 min at 4 °C. Supernatants were layered on a 10–50% sucrose gradient and spun at 230,000 × g for 2.5 h at 4 °C. Gradients were then fractionated while continuously monitoring absorbance at 254 nm. Total RNA was isolated from the fractions using TRIzol and the Direct-zol 96 RNA kit (Zymo Research) according to the manufacturer's instructions. cDNA was synthesized from 1 μg total RNA using the QuantiTect RT kit (Qiagen) according to manufacturer's instructions. qPCR was carried out using the ViiA7 qPCR system with *Taq*Man reagents using *Taq*Man primers/probes (Life Technologies) for *IFNB* and *HPRT*.

Virus infections.

Sindbis virus (SINV) was generated by electroporation of *in vitro* transcribed RNA from plasmid SINV TE/5′2J-GFP (from Dr. Charles Rice, Rockefeller University) into BHK cells as previously described[9]. For antiviral protection assays, SINV infections were performed in 24 well plates using MOI=0.1 and viral supernatants were harvested 16 h (for Huh7 cells) or 24 h (for Flp-In 293 cells) after infection and titrated on BHK cells. For immunofluorescence staining of SINV dsRNA intermediates, Huh7 cells were grown on collagen-coated glass coverslips and were infected with SINV Toto or AR86 at indicated MOIs in DMEM +10% FBS. At indicated time points, cells were washed once in PBS, fixed for 10 min in 4% PFA/PBS for 10 min at room temperature, and then incubated in 0.1% Triton X-100 for 10 min at room temperature. Coverslips were subsequently washed 3x in PBS before staining. Vesicular stomatitis virus (VSV) was a generous gift of J. Rose[46] and was propagated in BHK cells. VSV infections were performed in 24 well plates using a MOI=0.04 and viral supernatants were harvested 12 h after infection and titrated on BHK cells. For infection of Flp-In HEK 293T cells, doxycycline was added to 500 ng/ml 16 h before viral infection. For knockdown of ZAP isoforms in Huh7 cells prior to infection, siRNAs were transfected 16 h before infection. For Semliki Forest virus replicon assays, the vector pSMART was used[29], which expresses the non-structural proteins of Semliki Forest virus followed by a sub-genomic promoter driven beta-galactosidase protein. Expression of the beta-galactosidase gene is dependent on viral genome replication and expression of virally-transcribed genes. HEK 293T cells in 24 well plates were transfected with 200 ng pSMART and the indicated amount of pcDNA5/FRT/TO expressing ZAP constructs. After 24 h, cells were freeze/thawed three times and 4-methylumbelliferyl-β-D-galactopyranoside (4-MUG) was added to 200 μg/ml to measure beta-galactosidase activity. Fluorescence (excitation/emission wavelength of 365/460 nm) was monitored every 20 sec and the rate of fluorescence increase was averaged for 5 min.

Statistics.

Statistical analyses for quantitative assays were performed with Prism 8 (GraphPad Software) using Student’s t-test (to compare two conditions), one-way ANOVA with multiple comparisons (to compare more than two conditions), or two-way ANOVA with multiple comparisons (to compare between two independent variables) was performed to analyze statistical significance between treatment groups. The confidence interval for all statistical test was 95%. More information on analyses performed and exact P-values can be found in the legend of each Figure.

Data availability.

The data that support the findings of this study are available from the corresponding author upon reasonable request.

Supplementary Material

Refer to Web version on PubMed Central for supplementary material.

ACKNOWLEDGMENTS

This project was funded by National Institutes of Health grants AI108765 and AI135437 (R.S.), AI119017 and GM133633 (M.D.D.), AI104002, AI118916, AI127463 (M.G.), the Pew Biomedical Scholars program (M.D.D.), a Research Fellowship from the German Research Foundation (DFG) to J.S. (SCHW 1881/1-1), T32 training grants (AI106677 and GM007270) to F.W.S., and T32 training grant (GM007240) to A.P.R. This work was supported in part by the UW Proteomics Resource (UWPR95794). We would like to acknowledge P. von Haller and J. Eng (UW Proteomics Resource) for expert technical assistance with mass spectrometry. We are thankful for the support of W. P. Chang (UW Biology Imaging Facility) for help with super-resolution microscopy. We thank M. A. Davis (UW Immunology) for help with confocal laser scanning microscopy, D. B. Stetson and K. Burleigh (UW Immunology) for providing the *IRF3* CRISPR construct, S. N. Sarkar (University of Pittsburgh) for providing *STAT1* KO PH5CH8 cells, and members of the Savan, Daugherty and Gale labs for helpful discussions

REFERENCES

1. Schoggins JW et al. A diverse range of gene products are effectors of the type I interferon antiviral response. Nature 1 (2011).
2. Harris RS & Dudley JP APOBECs and virus restriction. Virology 479–480, 131–145 (2015).
3. Haller O, Staeheli P, Schwemmle M & Kochs G Mx GTPases: dynamin-like antiviral machines of innate immunity. Trends Microbiol 23, 154–163 (2015). [PubMed: 25572883]
4. Diamond MS & Farzan M The broad-spectrum antiviral functions of IFIT and IFITM proteins. Nat Rev Immunol 13, 46–57 (2013). [PubMed: 23237964]
5. Jarret A et al. Hepatitis-C-virus-induced microRNAs dampen interferon-mediated antiviral signaling. Nat Med 22, 1475–1481 (2016). [PubMed: 27841874]
6. McFarland AP et al. The favorable IFNL3 genotype escapes mRNA decay mediated by AU-rich elements and hepatitis C virus-induced microRNAs. Nat Immunol 15, 72–79 (2014). [PubMed: 24241692]
7. Savan R Post-transcriptional regulation of interferons and their signaling pathways. Journal of interferon & cytokine research : the official journal of the International Society for Interferon and Cytokine Research 34, 318–329 (2014).
8. Schwerk J & Savan R Translating the Untranslated Region. J Immunol 195, 2963–2971 (2015). [PubMed: 26386038]
9. Bick MJ et al. Expression of the Zinc-Finger Antiviral Protein Inhibits Alphavirus Replication. Journal of Virology 77, 11555–11562 (2003). [PubMed: 14557641]
10. Gao G, Guo X & Goff SP Inhibition of retroviral RNA production by ZAP, a CCCH-type zinc finger protein. Science 297, 1703–1706 (2002). [PubMed: 12215647]
11. Muller S et al. Inhibition of filovirus replication by the zinc finger antiviral protein. J Virol 81, 2391–2400 (2007). [PubMed: 17182693]
12. Zhu Y et al. Zinc-finger antiviral protein inhibits HIV-1 infection by selectively targeting multiply spliced viral mRNAs for degradation. Proceedings of the National Academy of Sciences 108, 15834–15839 (2011).
13. Guo X, Carroll JW, Macdonald MR, Goff SP & Gao G The zinc finger antiviral protein directly binds to specific viral mRNAs through the CCCH zinc finger motifs. J Virol 78, 12781–12787 (2004). [PubMed: 15542630]
14. Guo X, Ma J, Sun J & Gao G The zinc-finger antiviral protein recruits the RNA processing exosome to degrade the target mRNA. Proc Natl Acad Sci U S A 104, 151–156 (2007). [PubMed: 17185417]
15. Kerns JA, Emerman M & Malik HS Positive selection and increased antiviral activity associated with the PARP-containing isoform of human zinc-finger antiviral protein. PLoS genetics 4, e21 (2008). [PubMed: 18225958]
16. Vyas S, Chesarone-Cataldo M, Todorova T, Huang YH & Chang P A systematic analysis of the PARP protein family identifies new functions critical for cell physiology. Nat Commun 4, 2240 (2013). [PubMed: 23917125]
17. Hayakawa S et al. ZAPS is a potent stimulator of signaling mediated by the RNA helicase RIG-I during antiviral responses. Nat Immunol 12, 37–44 (2011). [PubMed: 21102435]

18. Ryman KD et al. Sindbis virus translation is inhibited by a PKR/RNase L-independent effector induced by alpha/beta interferon priming of dendritic cells. J Virol 79, 1487–1499 (2005). [PubMed: 15650175]
19. Wang N et al. Viral induction of the zinc finger antiviral protein is IRF3-dependent but NF-kappaB-independent. The Journal of biological chemistry 285, 6080–6090 (2010). [PubMed: 20048147]
20. Takagaki Y, Seipelt RL, Peterson ML & Manley JL The polyadenylation factor CstF-64 regulates alternative processing of IgM heavy chain pre-mRNA during B cell differentiation. Cell 87, 941–952 (1996). [PubMed: 8945520]
21. Chuvpilo S et al. Alternative polyadenylation events contribute to the induction of NFATc in effector T cells. Immunity 10, 261–269 (1999). [PubMed: 10072078]
22. Shell SA, Hesse C, Morris SM Jr. & Milcarek C Elevated levels of the 64-kDa cleavage stimulatory factor (CstF-64) in lipopolysaccharide-stimulated macrophages influence gene expression and induce alternative poly(A) site selection. The Journal of biological chemistry 280, 39950–39961 (2005). [PubMed: 16207706]
23. Lee H et al. Zinc-finger antiviral protein mediates retinoic acid inducible gene I-like receptor-independent antiviral response to murine leukemia virus. Proc Natl Acad Sci U S A 110, 12379–12384 (2013). [PubMed: 23836649]
24. Charron G, Li MM, MacDonald MR & Hang HC Prenylome profiling reveals S-farnesylation is crucial for membrane targeting and antiviral activity of ZAP long-isoform. Proc Natl Acad Sci U S A 110, 11085–11090 (2013). [PubMed: 23776219]
25. Wang M & Casey PJ Protein prenylation: unique fats make their mark on biology. Nat Rev Mol Cell Biol 17, 110–122 (2016). [PubMed: 26790532]
26. Gustafsson MG Surpassing the lateral resolution limit by a factor of two using structured illumination microscopy. J Microsc 198, 82–87 (2000). [PubMed: 10810003]
27. Zhang Y, Burke CW, Ryman KD & Klimstra WB Identification and characterization of interferon-induced proteins that inhibit alphavirus replication. J Virol 81, 11246–11255 (2007). [PubMed: 17686841]
28. Kujala P et al. Biogenesis of the Semliki Forest virus RNA replication complex. J Virol 75, 3873–3884 (2001). [PubMed: 11264376]
29. DiCiommo DP & Bremner R Rapid, high level protein production using DNA-based Semliki Forest virus vectors. The Journal of biological chemistry 273, 18060–18066 (1998). [PubMed: 9660762]
30. Chiu HP et al. Inhibition of Japanese encephalitis virus infection by the host zinc-finger antiviral protein. PLoS Pathog 14, e1007166 (2018). [PubMed: 30016363]
31. Zhu Y & Gao G ZAP-mediated mRNA degradation. RNA Biol 5, 65–67 (2008). [PubMed: 18418085]
32. Zhu Y, Wang X, Goff SP & Gao G Translational repression precedes and is required for ZAP-mediated mRNA decay. EMBO J 31, 4236–4246 (2012). [PubMed: 23023399]
33. Rosengren AT, Nyman TA, Syyrakki S, Matikainen S & Lahesmaa R Proteomic and transcriptomic characterization of interferon-alpha-induced human primary T helper cells. Proteomics 5, 371–379 (2005). [PubMed: 15700245]
34. Huang Z, Wang X & Gao G Analyses of SELEX-derived ZAP-binding RNA aptamers suggest that the binding specificity is determined by both structure and sequence of the RNA. Protein Cell 1, 752–759 (2010). [PubMed: 21203916]
35. Takata MA et al. CG dinucleotide suppression enables antiviral defence targeting non-self RNA. Nature 550, 124–127 (2017). [PubMed: 28953888]
36. Chen S et al. Structure of N-terminal domain of ZAP indicates how a zinc-finger protein recognizes complex RNA. Nat Struct Mol Biol 19, 430–435 (2012). [PubMed: 22407013]
37. Glasker S, Toller M & Kummerer BM The alternate triad motif of the poly(ADP-ribose) polymerase-like domain of the human zinc finger antiviral protein is essential for its antiviral activity. J Gen Virol 95, 816–822 (2014). [PubMed: 24457973]

38. Liu CH, Zhou L, Chen G & Krug RM Battle between influenza A virus and a newly identified antiviral activity of the PARP-containing ZAPL protein. Proc Natl Acad Sci U S A 112, 14048–14053 (2015). [PubMed: 26504237]

39. Wang XL et al. Sindbis Virus Can Exploit a Host Antiviral Protein To Evade Immune Surveillance. Journal of Virology 90, 10247–10258 (2016). [PubMed: 27581990]

METHODS-ONLY REFERENCES

40. Saito T, Owen DM, Jiang F, Marcotrigiano J & Gale M Jr. Innate immunity induced by composition-dependent RIG-I recognition of hepatitis C virus RNA. Nature 454, 523–527 (2008). [PubMed: 18548002]

41. Urban TJ et al. IL28B genotype is associated with differential expression of intrahepatic interferon-stimulated genes in patients with chronic hepatitis C. Hepatology 52, 1888–1896 (2010). [PubMed: 20931559]

42. Friedman JR, Webster BM, Mastronarde DN, Verhey KJ & Voeltz GK ER sliding dynamics and ER-mitochondrial contacts occur on acetylated microtubules. J Cell Biol 190, 363–375 (2010). [PubMed: 20696706]

43. Rowland AA, Chitwood PJ, Phillips MJ & Voeltz GK ER contact sites define the position and timing of endosome fission. Cell 159, 1027–1041 (2014). [PubMed: 25416943]

44. Olenych SG, Claxton NS, Ottenberg GK & Davidson MW The fluorescent protein color palette. Curr Protoc Cell Biol Chapter 21, Unit 21 25 (2007).

45. Vogt DA & Ott M Membrane Flotation Assay. Bio Protoc 5 (2015).

46. Boritz E, Gerlach J, Johnson JE & Rose JK Replication-competent rhabdoviruses with human immunodeficiency virus type 1 coats and green fluorescent protein: entry by a pH-independent pathway. J Virol 73, 6937–6945 (1999). [PubMed: 10400792]

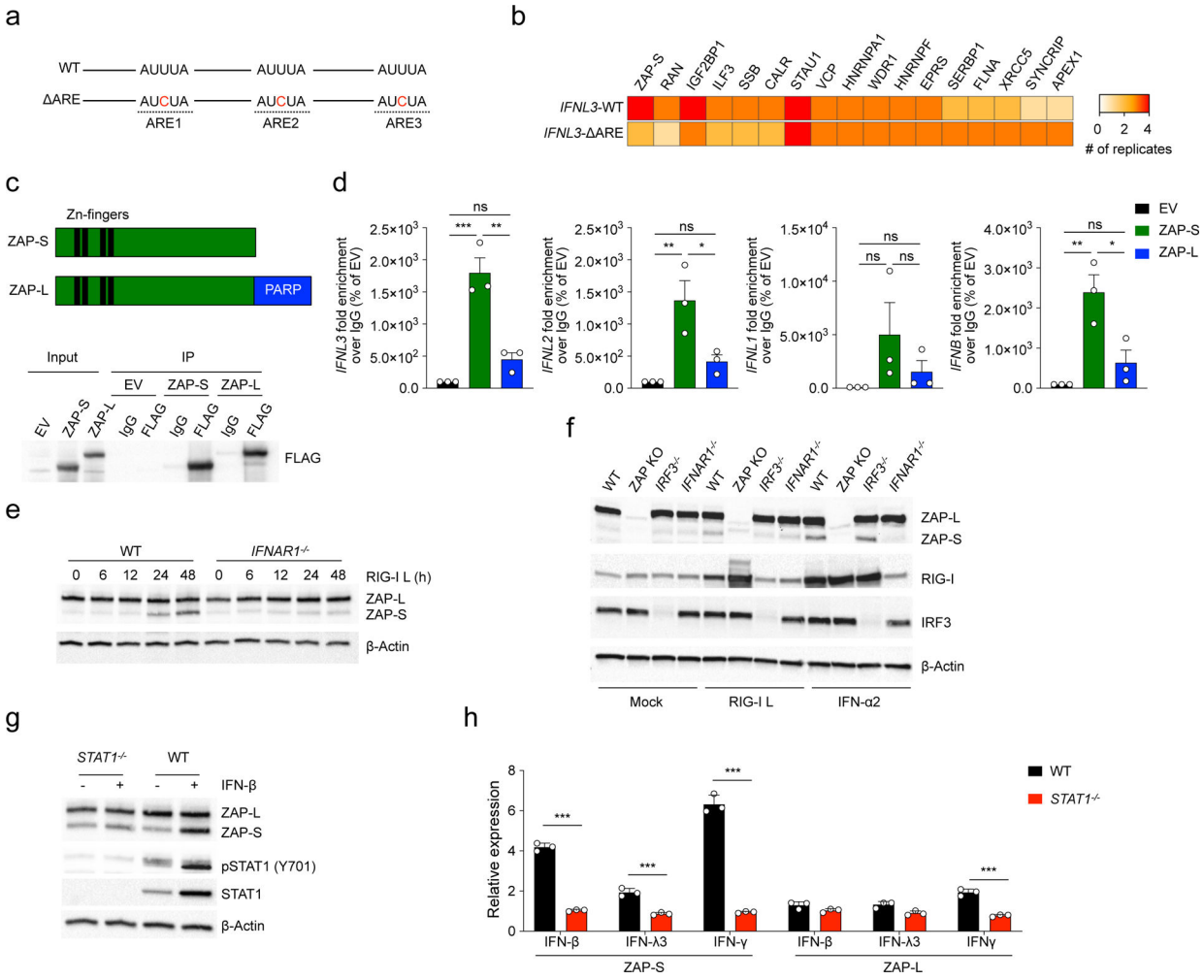

Figure 1. ZAP-S interacts with the 3′UTR of *IFN* mRNAs.

(a) Schematic of *IFNL1*, *IFNL2* and *IFNL3* 3′UTR sequences showing AREs 1–3 and mutations (ATTTA > ATCTA) introduced to disrupt the motifs (ΔARE). (b) Mass spectrometry of biotinylated *IFNL3* 3′UTR and interacting proteins of HepG2 cell lysate. (c) Domain structures of ZAP-S and ZAP-L protein isoforms. Western blot of immunoprecipitated FLAG-tagged ZAP-S, ZAP-L and empty vector (EV) control in Huh7 ZAP KO cells 24 h after stimulation with poly U/UC RNA. (d) qPCR analysis of immunoprecipitated FLAG-tagged ZAP-S, ZAP-L and empty vector (EV) control in Huh7 ZAP KO cells after stimulation with poly U/UC RNA for 24 h. Data from three independent experiments is shown combined as fold enrichment over IgG control (% of EV). Bars show mean ± SEM. (e) Western blot of ZAP isoform expression in Huh7 WT and *IFNAR1*$^{-/-}$ cells after stimulation with 0.3 μg/ml poly U/UC RNA (RIG-I L). (f) Western blot of ZAP isoform expression in Huh7 wild-type, ZAP KO, *IFNAR1*$^{-/-}$ and *IRF3*$^{-/-}$ cells after stimulation with 0.2 μg/ml poly U/UC RNA (RIG-I L) or treatment with 100 ng/ml recombinant human IFN-α2 for 48 h. (g) Western blot of ZAP isoform expression in PH5CH8 wild-type and *STAT1* cells after treatment with 200 IU/ml IFN-β for 24 h. (h) qPCR of ZAP isoform mRNA expression in PH8CH8 wild-type and *STAT1*$^{-/-}$ cells after treatment with 25 IU/ml IFN-β, 100 ng/ml IFN-λ3 or 5 ng/ml IFN-γ for 9 h. Data shown is

representative of three independent experiments with replicates (n=3) and similar results. Bars show mean ± SD. (c, e-g) Representative Western blots of three individual experiments with similar results are shown. Data were analyzed using (d) one-way ANOVA with Tukey's post-test or (h) two-way ANOVA with Sidak's post-test. *$P < 0.05$; **$P < 0.01$; ***$P < 0.001$; ns, not significant.

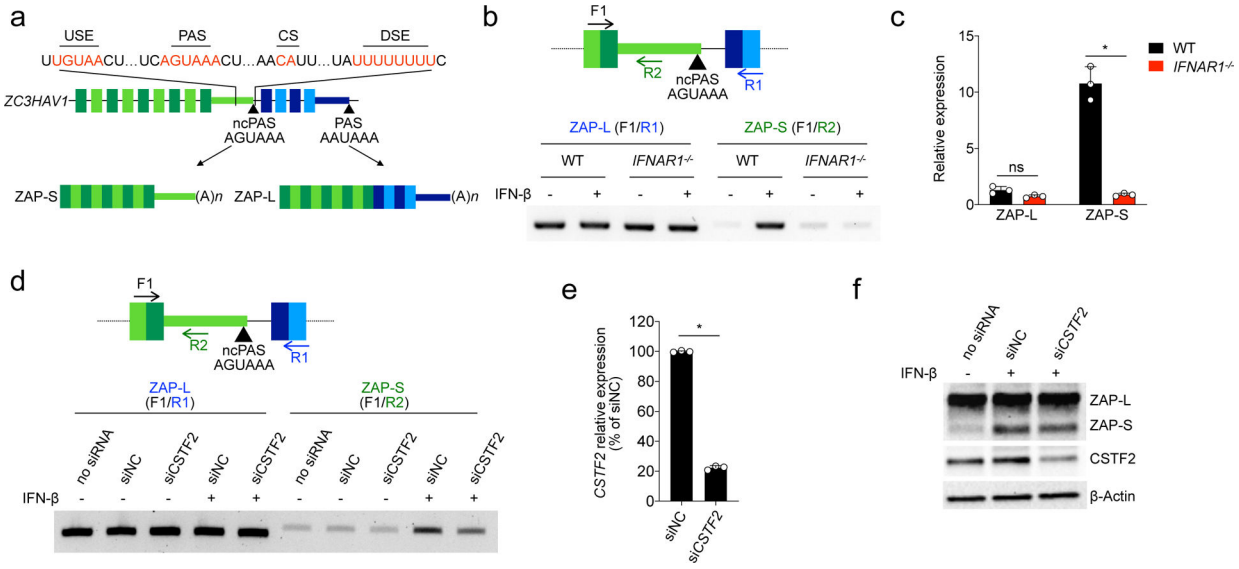

Figure 2. CSTF2-mediated alternative polyadenylation generates ZAP-S.

(a) Schematic of intron/exon structure of the *ZC3HAV1* gene. The intron between exons 9 and 10 harbors a non-canonical weak polyadenylation signal (ncPAS, AGUAAA) that is flanked by an upstream element (USE) and a downstream element (DSE) required for recruitment of the 3′ processing machinery. (b) PCR on cDNA of Huh7 wild-type and *IFNAR1*$^{-/-}$ cells stimulated with or without 250 IU/ml IFN-β for 8 h. (c) qPCR with ZAP isoform-specific probes on cDNA of Huh7 wild-type and *IFNAR1*$^{-/-}$ cells stimulated with or without 250 IU/ml IFN-β for 8 h. (d) PCR on cDNA of Huh7 WT cells transfected with non-targeting control (NC) or *CSTF2* siRNA and stimulated for 24 h with or without 250 IU/ml IFN-β 24 h after siRNA transfection. (e) *CSTF2* mRNA expression in Huh7 cells upon knockdown of *CSTF2* and stimulation with 250 IU/ml IFN-β for 24 h. (f) Western blot of ZAP protein expression in Huh7 cells upon knockdown of *CSTF2* and stimulation with 250 IU/ml IFN-β for 24 h. (b-f) Data shown are representative of three independent experiments with replicates (n=3) and similar results. Bars show mean ± SD. Data were analyzed using (c) two-way ANOVA with Sidak's post-test or (e) unpaired two-tailed Student's t-test. *$P < 0.001$; ns, not significant.

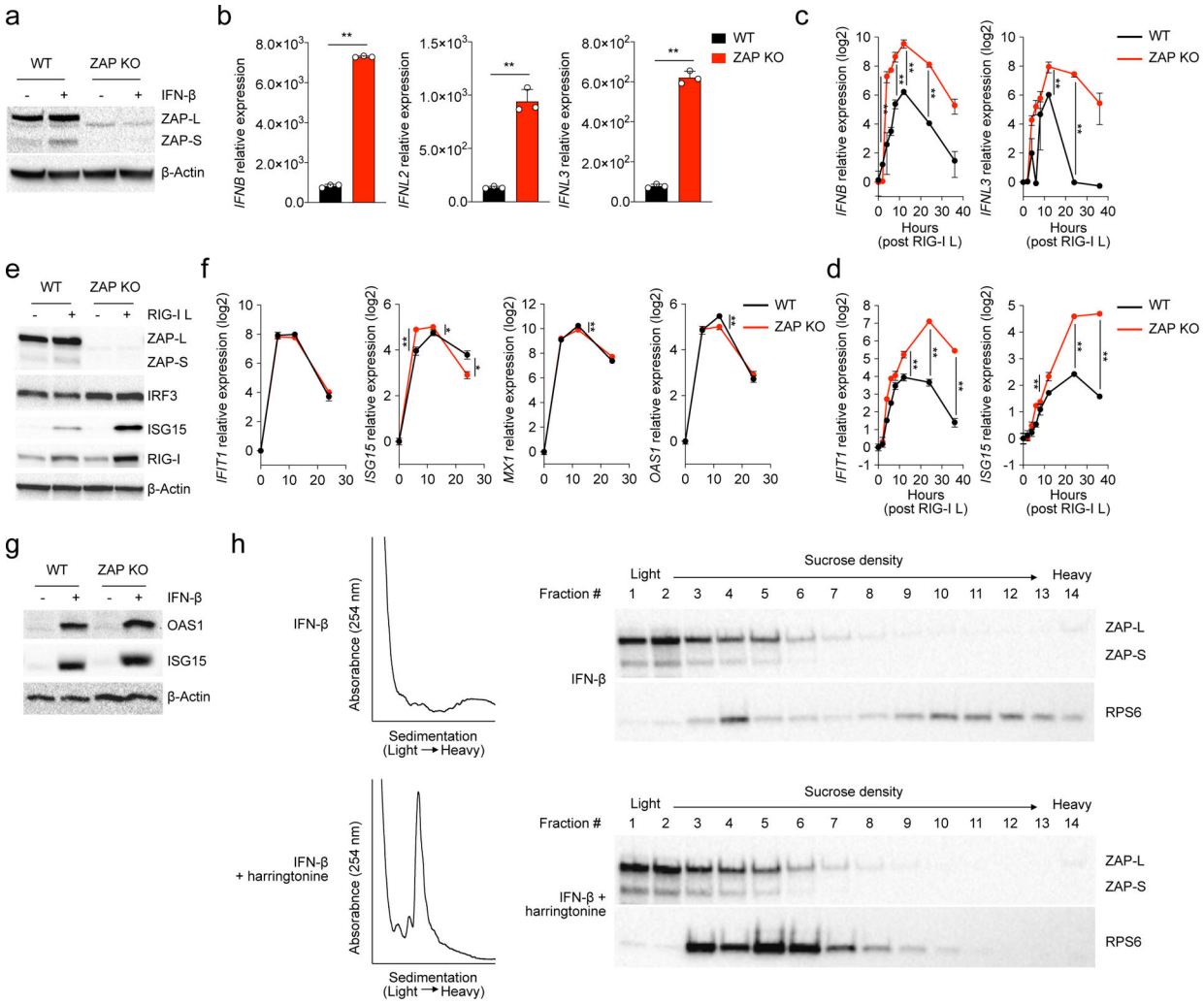

Figure 3. ZAP-deficient cells have a higher and more prolonged IFN response.

(a) Western blot of Huh7 wild-type and ZAP KO cells treated with IFN-β for 24 h. (b) Expression of *IFNB*, *IFNL2* and *IFNL3* mRNA in Huh7 wild-type and ZAP KO cells 18 h after stimulation with poly U/UC RNA. Bars show mean ± SD. (c, d) Time course of (c) *IFNB* and *IFNL3* mRNA or (d) *IFIT1* and *ISG15* mRNA expression upon pulsing of Huh7 wildtype and ZAP KO cells with 1 μg/ml poly U/UC RNA (RIG-I L) for 2 h. Symbols show mean ± SD. (e) Western blot of ZAP, IRF3, ISG15 and RIG-I protein expression in Huh7 wild-type and ZAP KO cells 36 h after stimulation with 0.2 μg/ml poly U/UC RNA (RIG-I L). (f) Expression of *IFIT1*, *ISG15*, *MX1* and *OAS1* mRNA upon treatment of Huh7 wild-type and ZAP KO cells with 25 IU/ml IFN-β. Symbols show mean ± SD. (g) Western blot of ISG15 and OAS1 protein expression in Huh7 wild-type and ZAP KO cells after stimulation with 25 IU/ml IFN-β for 24 h. (h) Polysome fractionation of Huh7 wild-type cells treated with 500 IU/ml IFN-β for 24 h, and with or without 5 μg/ml harringtonine. In (a-h) data shown is representative of three independent experiments with replicates (n=3) for (b-d, f) and similar results. Data were analyzed using (b) unpaired two-tailed Student's t-test or (c, d, f) two-way ANOVA with Sidak's post-test. *$P < 0.01$; **$P < 0.001$.

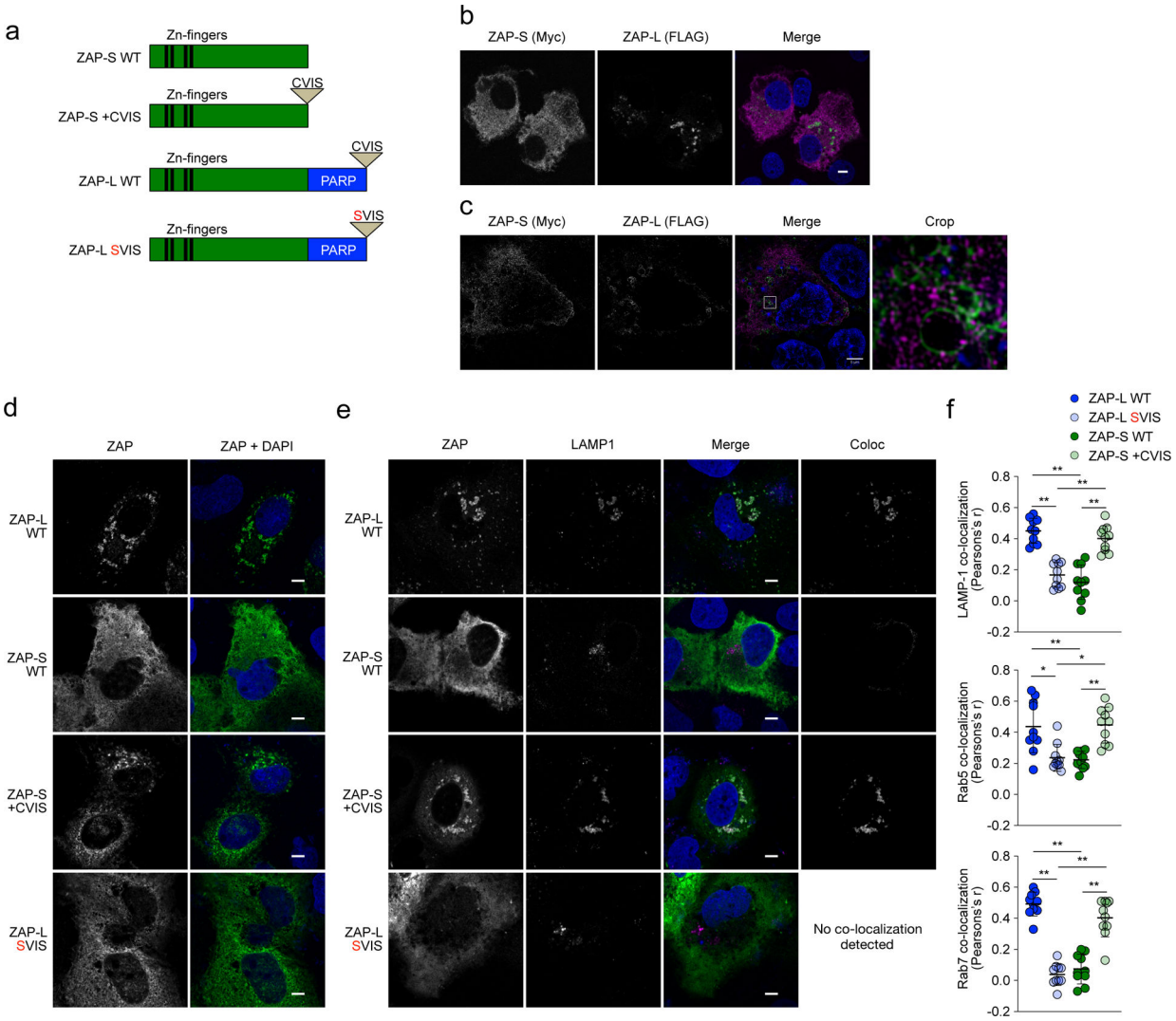

Figure 4. ZAP-S and ZAP-L localize to different subcellular compartments.

(a) Schematic of WT ZAP-S and WT ZAP-L and their CaaX motif (CVIS) mutants generated by site-directed mutagenesis. (b) Confocal immunofluorescence microscopy of Myc-tagged ZAP-S and FLAG-tagged ZAP-L upon co-expression in Huh7 ZAP KO cells. The scale bar represents 5 μm. (c) Super-resolution structured illumination microscopy (SIM) of Myc-tagged ZAP-S and FLAG-tagged ZAP-L co-expressed in Huh7 ZAP KO cells. (d) Confocal immunofluorescence microscopy of tagless WT ZAP-S, WT ZAP-L, or their respective CaaX motif mutants upon expression in Huh7 ZAP KO cells. The scale bar represents 5 μm. (e) Confocal immunofluorescence microscopy of ZAP and LAMP1 upon co-expression of mCherry-LAMP1 and tagless WT ZAP-S and WT ZAP-L, or their CaaX motif mutants. The scale bar represents 5 μm. For (b-e) representative micrographs of three independently performed experiments are depicted. (f) Quantification of co-localization of ZAP with LAMP1-, Rab5-, and Rab7-positive pixels. The correlation coefficients (Pearson's r) of cells (n=10) from two independent experiments are shown and were calculated using the Fiji Coloc 2 plugin and one-way ANOVA with Tukey's post-test. Error bars show mean ± SD. *$P < 0.01$; **$P < 0.001$.

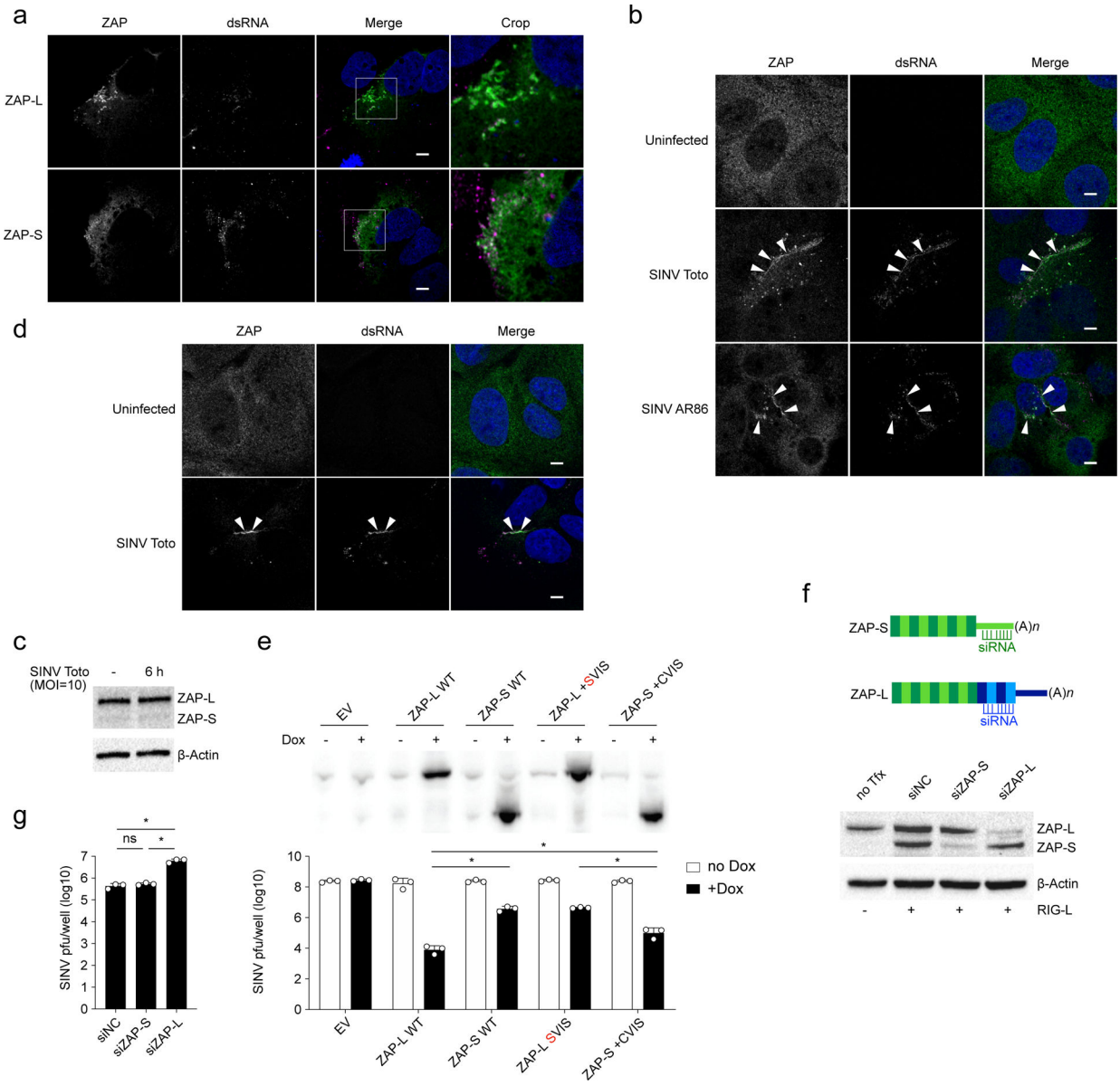

Figure 5. ZAP-L targets alphavirus RNA at viral replication sites.

(a) Confocal immunofluorescence microscopy of ZAP and SINV dsRNA in Huh7 ZAP KO cells expressing WT ZAP-L or WT ZAP-S 6 hpi with SINV Toto (MOI=10). The scale bar represents 5 μm. (b) Confocal immunofluorescence microscopy of endogenous ZAP and SINV (strains Toto and AR86) dsRNA 6 hpi of Huh7 wild-type cells (MOI=10). (c) Western blot of endogenous ZAP isoform expression in Huh7 wild-type cells 6 hpi with SINV Toto (MOI=10). (d) Confocal immunofluorescence microscopy of ZAP and viral dsRNA in Huh7 *IRF3*$^{-/-}$ cells 6 hpi with SINV Toto (MOI=10). The scale bar represents 5 μm. (e) Viral titers from doxycycline-inducible HEK 293T cells expressing WT ZAP-S, WT ZAP-L or their respective CaaX motif mutants 24 hpi with SINV (MOI=0.1). Bars show mean ± SD. Data is representative of three independently performed experiments with replicates (n=3) and similar results. (f) Schematic of ZAP isoform-specific siRNA design and Western blot of

ZAP isoform expression showing specificity of siRNAs. (g) Viral titers after siRNA-mediated knockdown of endogenous ZAP-S or ZAP-L in Huh7 wild-type cells 16 hpi with SINV (MOI=0.1). Bars show mean ± SD. Data is representative of three independently performed experiments with replicates (n=3) and similar results. For (a-d, f) representative micrographs and Western blots of three independently performed experiments with similar results are depicted. Data were analyzed using (e) two-way ANOVA with Sidak's post-test or (g) one-way ANOVA with Tukey's post-test. *$P < 0.001$; ns, not significant.

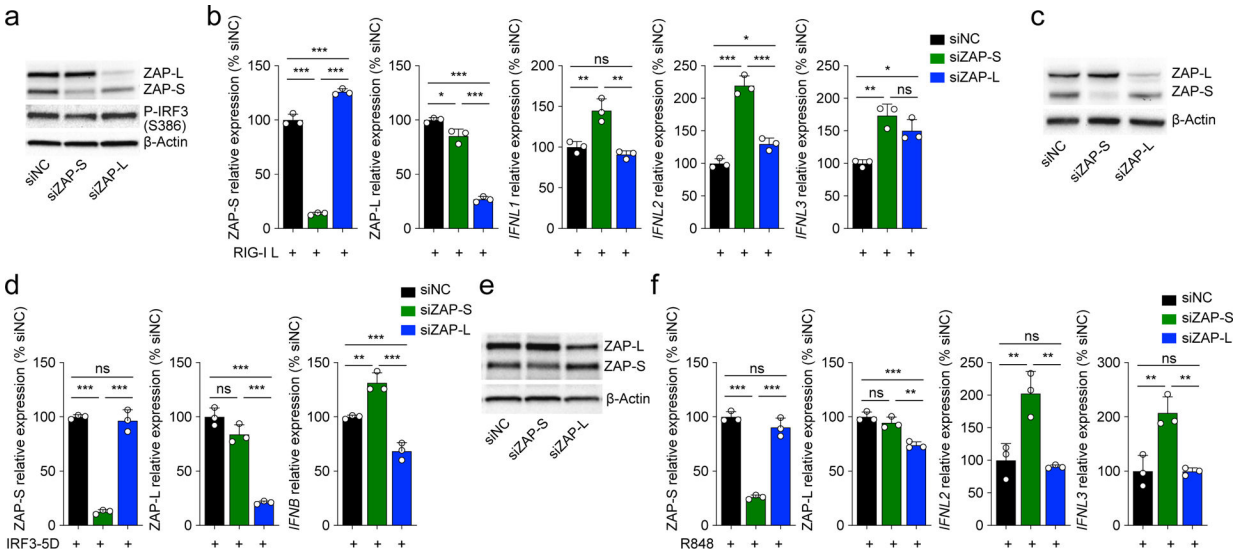

Figure 6. ZAP-S, but not ZAP-L, suppresses IFN.

(a) Western blot of ZAP isoform expression and (b) *ZAP-S*, *ZAP-L*, *IFNB*, *IFNL2* and *IFNL3* mRNA expression in Huh7 wild-type cells after isoform-specific knockdown of ZAP and stimulation with 0.5 μg/ml poly U/UC RNA (RIG-I L) for 42 h. Bars show mean ± SD. (c) Western blot of ZAP isoform expression and (d) *ZAP-S*, *ZAP-L* and *IFNB* mRNA expression in Huh7 wild-type cells after isoform-specific knockdown of ZAP and overexpression of IRF3–5D for 42 h. Bars show mean ± SD. (e) Western blot of ZAP isoform expression and (f) *ZAP-S*, *ZAP-L*, *IFNL2* and *IFNL3* mRNA expression in CAL-1 cells after isoform-specific knockdown of ZAP and stimulation with 1 μg/ml R848 for 3 h. Bars show mean ± SD. For (a-f) data is representative of three independently performed experiments with replicates (n=3) and similar results. Data were analyzed using one-way ANOVA with Tukey's post-test. *$P < 0.05$; **$P < 0.01$; ***$P < 0.001$; ns, not significant.

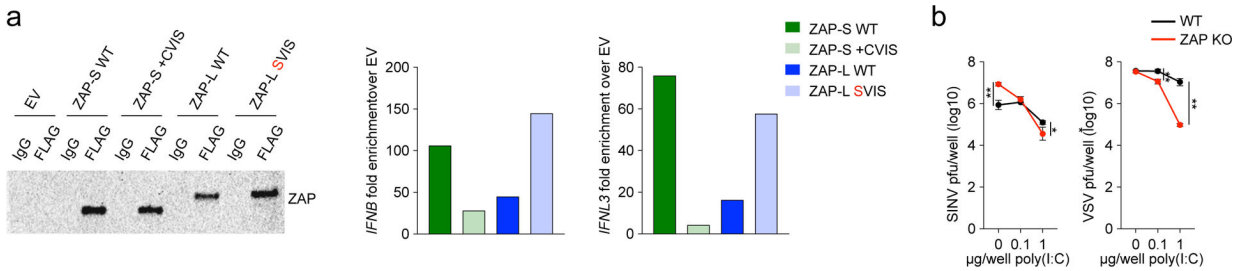

Figure 7. Localization of ZAP isoforms determines binding of *IFN* mRNA.

(a) RNA immunoprecipitation of FLAG-tagged WT ZAP-S, WT ZAP-L, their respective CaaX mutants, and empty vector (EV) control in Huh7 ZAP KO cells after stimulation with 0.25 µg/ml poly U/UC RNA for 24 h. A representative experiment of three independent experiments with similar results is shown. (b) SINV titers 16 hpi and Vesicular stomatitis virus (VSV) titers 12 hpi in Huh7 wild-type and ZAP KO cells with or without poly(I:C) pre-treatment for 16 h. Symbols show mean ± SD. Data is representative of three independently performed experiments with replicates (n=3). Data were analyzed using two-way ANOVA with Tukey's post-test. $*P < 0.01$; $**P < 0.001$.

Table 1.

Overview of ZAP co-localization with different cell organelles.

Organelle	Marker	ZAP-S WT	ZAP-L WT	ZAP-S +CVIS	ZAP-L SVIS
Early endosome	Rab5	no	yes	yes	no
Late endosome	Rab7	no	yes	yes	no
Lysosome	LAMP1	no	yes	yes	no
Mitochondria	COX8	no	no	no	no
Endoplasmic reticulum	Sec61β	no	no	no	no
Peroxisomes	PTS1	no	no	no	no